



A study of cosmic microwave background using non-extensive statistics

Somita Dhal¹ · R. K. Paul¹

Received: 22 February 2024 / Accepted: 27 May 2024 / Published online: 12 June 2024
© The Author(s), under exclusive licence to Springer Nature B.V. 2024

Abstract

The cosmic microwave background (CMB) radiation, the relic afterglow of the Big Bang, has become one of the most useful and precise tools in modern precision cosmology. In this article, we employ Tsallis non-extensive statistical framework to calculate the cosmic microwave background (CMB) temperature and its probability distribution by utilising a recently proposed blackbody radiation inversion (BRI) technique and the cosmic background explorer/ far infrared absolute spectrophotometer (COBE/FIRAS) dataset. Here, we have used the best-fit values of $q=0.99888 \pm 0.00016$ and $q=1.00012 \pm 0.00001$, obtained by fitting COBE/FIRAS data with two different versions of non-extensive models. We compare the results with the more conventional extensive statistical analysis i.e. for $q=1$.

Keywords Non-extensive statistics · COBE/FIRAS · Blackbody Radiation Inversion · Cosmic Microwave Background · Temperature fluctuations

1 Introduction

In 1965, Robert Wilson and Arno Penzias made the significant discovery of cosmic microwave background (CMB) radiation, nearly uniform radiation found in all directions [1]. Several studies have provided a detailed history of the cosmic microwave background radiation's prediction and detection [2–5]. The detection of CMB radiation marks a crucial milestone in the Big Bang model of the universe, as it offers a compelling explanation for the remnants from the early cosmos. The presence of this radiation must be considered in all proposed universe models, making the cosmic microwave background an essential tool for precise cosmological measurements [6, 7]. The COBE satellite has played a pivotal role in advancing the field of cosmology by achieving remarkable accomplishments [8–11].

✉ R. K. Paul
ratan_bit1@rediffmail.com

¹ Birla Institute of Technology, Mesra, Ranchi 835215, Jharkhand, India

In the context of the early universe, non-extensive statistics have been considered a possible framework to describe the thermodynamic properties of the universe during certain phases. The concept of non-extensive statistics, proposed by physicist Constantino Tsallis, suggests a generalisation of the standard Boltzmann-Gibbs statistics, which describes systems with long-range interactions and non-additive entropy [12–14]. Till now, researchers have used non-extensive thermostatics to explore a range of physical systems, including two-dimensional turbulence, linear response theory, the solar neutrino problem, and the characteristics of black holes [15–20]. Also, non-extensive statistical mechanics have been applied to the CMB spectrum for the investigation of modification of dipole anisotropy and S-Z effect [21].

Departures from the ideal conditions in the early universe left their imprints in the cosmic microwave background radiation, which are observed as tiny anisotropies in an otherwise isotropic radiation. The standard cosmological theory suggests that the origin of these fluctuations is the underlying gravitational inhomogeneities. This gravitational interaction results in a non-extensive situation because of the divergence in the partition function [22]. Hence, studying the CMB temperature and its fluctuations within a non-extensive framework is better suited. Here, we use Tsallis statistics with the index ‘ q ’. As pointed out in [23], $|q - 1|$ has a tight constraint of 10^{-5} . This sets our goal to compute the relative differences of the models by varying ‘ q ’.

Here, to investigate the parameters of CMB radiation, we used the data sets of COBE/FIRAS, which reflects the relationship between the frequency and intensity of the CMB spectrum [24]. This paper aims to calculate the parameters (i.e., temperature and uncertainty) of CMB radiation within the framework of non-extensive statistical mechanics, employing the formulation of blackbody radiation inversion (we used the concept of mixing black bodies [25]). An essential aspect of this research involves comparing the results obtained using two different ways of analysing statistics: extensive ($q=1$) and non-extensive ($q \neq 1$) cases. q is the non-extensive index. This comparison aims to understand the deviation of results from standard Boltzmann statistics ($q=1$). The solution to the blackbody radiation inversion (BRI) problem involves comparing the observed radiation spectrum (COBE/FIRAS data) of an object with the theoretical spectrum (our approach) of black bodies at different temperatures. The process of solving the blackbody radiation inversion problem is explained in detail in Sect. 2.

We have investigated three cases: (i) generalised energy density per unit frequency [26], (ii) generalised Planck’s radiation law by C. Tsallis [27], and (iii) Standard Planck’s law ($q=1$). These two formulas are fitted to experimental data [24] to find the value of q , T and the best-fit value of q is used for further calculation. Here, we took two non-extensive cases, i.e., different q values. Additionally, we reconstruct the intensity of the CMB spectrum evidencing our methodology. The Probability distribution functions for $q=1$ (i.e., Boltzmann-Gibbs’s statistics) and $q \neq 1$ are compared.

This paper is comprised of five sections. Section 2 represents the methodology for calculating the best-fit value of the q , T from two different generalised Planck’s formula and application of the BRI technique, Sect. 3 represents the results, Sect. 4 reflects the comparison of all the probability values, and Sect. 5 compromises the discussion of results.

2 Methodology

We have investigated the monopole temperature and fluctuation in temperature of CMB for three cases: (a) For generalised Planck’s law in terms of energy density (we have calculated the intensity from energy density using $I = \frac{U \times c}{4\pi}$; c is the velocity of light), (b) non-extensive Intensity formula for Planck’s distribution by C. Tsallis, and (c) for Planck’s law ($q=1$).

Curve fitting is a commonly used method for finding a mathematical function closely matching a given dataset. This technique can be applied in various situations, such as determining the overall pattern in collected data, isolating data from noisy backgrounds, and extracting specific parameters from the curve. In our case, we focus on the third application mentioned. By choosing q , T (CMB monopole temperature) as an unknown parameter and using the experimental data from the source [24], we calculate the value of q , T as the best-fit parameter by fitting Eqs. (1) and (2) as the mathematical function. The obtained fit is depicted in Figs. 1 and 2, respectively. The value of q will be used in further calculations.

2.1 Determining the best-fit values for q and T

In this section, we analyse the data obtained from the COBE satellite and compare it to the modified generalised intensity equation within the framework of non-extensive thermostatics [26]. The experimental data used for this analysis can be found on the NASA website [24]. The main objective of this analysis is to determine the best-fit values for q and T that provide the best fit.

The generalised energy density for unit frequency is given as (refer to Eq. 26 of reference [26]).

$$U(\nu, q, T) = \frac{8\pi h\nu^3 q e^{(2q-1)\frac{h\nu}{kT}} - e^{(q-1)\frac{h\nu}{kT}}}{c^3 \left\{ e^{(2q-1)\frac{h\nu}{kT}} - 1 \right\}^2} \tag{1}$$

From Eq. (1) the spectral radiance can be written as.

$$I_1(\nu, q, T) = \frac{2h\nu^3 q e^{(2q-1)\frac{h\nu}{kT}} - e^{(q-1)\frac{h\nu}{kT}}}{c^2 \left\{ e^{(2q-1)\frac{h\nu}{kT}} - 1 \right\}^2} \tag{2}$$

where h is Planck’s constant, ν is the frequency, k is the Boltzmann constant, T is the temperature of CMB, q is the non-extensivity parameter (entropy index), and I_1 is the spectral radiance. The parameter ‘ q ’ in the context of Tsallis statistics plays a crucial role in characterising the departure from classical statistical mechanics, particularly the Boltzmann-Gibbs statistics.

Above Fig. 1 exhibits an exceptional agreement with the COBE/FIRAS outcome, indicated by a favourable χ^2/dof value of approximately 1 and a T value consistent with the literature. This motivates us to explore a more coherent scenario by considering a non-extensive formulation of Planck’s distribution, represented by Eq. 5.

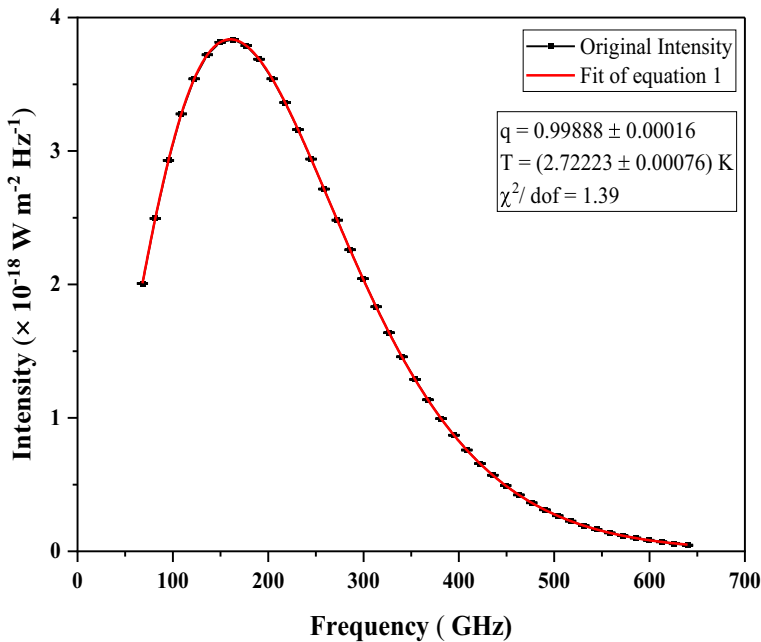


Fig. 1 Fitting Eq. 2 with experimental data with error bars(1σ) is shown. The value of $\chi^2/\text{dof}=56.99/41=1.39$ (95% confidence level) offers a good fitting. The fitting value of q is found to be 0.99888 ± 0.00016 . The value of T found from best fit is $T = (2.72223 \pm 0.00076)$ K consistent with the literature (i.e., $T=2.72548 \pm 0.00057$) [28]

Dof refers to the degrees of freedom. The degrees of freedom depend on the number of parameters we are estimating in a model. In our case, we are estimating q and T by fitting an equation to the original COBE data. Since the original dataset consists of 43 data points, so there are 41 degrees of freedom.

The expression for photon density per unit volume was originally introduced by Tsallis in 1995 within the framework of non-extensive statistics (refer to Eq. 15 of reference [27]). This formula generalises Planck’s law for blackbody radiation by incorporating the parameter q , which characterises non-extensive behaviour. It can be represented as

$$D_q(\nu) \sim D_{\text{Planck}}(\nu) \left(1 - e^{-\frac{h\nu}{kT}}\right)^{q-1} \left[1 + (1 - q) \frac{h\nu}{kT} \left\{ \frac{1 + e^{-\frac{h\nu}{kT}}}{1 - e^{-\frac{h\nu}{kT}}} - \frac{\frac{h\nu}{kT}}{2} \frac{1 + 3e^{-\frac{h\nu}{kT}}}{\left(1 - e^{-\frac{h\nu}{kT}}\right)^2} \right\} \right] \tag{3}$$

In subsequent work by Biyajima et al. in 2012 [29], energy density for Planck’s radiation was derived from Eq. 3 in the non-extensive framework. For $|q - 1| \ll 1$ for energy density per unit frequency can be approximated as

$$U(\nu, q, T) = U_{\text{Planck}}(\nu, T) + \frac{8\pi h\nu^3}{c^3} \frac{q-1}{e^{\frac{h\nu}{kT}} - 1} \left\{ \ln\left(1 - e^{-\frac{h\nu}{kT}}\right) - \frac{h\nu}{kT} \frac{1 + e^{-\frac{h\nu}{kT}}}{1 - e^{-\frac{h\nu}{kT}}} + \frac{\left(\frac{h\nu}{kT}\right)^2}{2} \frac{1 + 3e^{-\frac{h\nu}{kT}}}{\left(1 - e^{-\frac{h\nu}{kT}}\right)^2} \right\} \tag{4}$$

Where $U_{\text{Planck}}(\nu, T) = \frac{8\pi h\nu^3}{c^3} \frac{1}{e^{\frac{h\nu}{kT}} - 1}$

From Eq. 4 the spectral radiance can be written as.

$$I_2(\nu, q, T) = \frac{2h\nu^3}{c^2} \frac{1}{e^{\frac{h\nu}{kT}} - 1} \left[1 + (q-1) \left\{ \ln\left(1 - e^{-\frac{h\nu}{kT}}\right) - \frac{h\nu}{kT} \frac{1 + e^{-\frac{h\nu}{kT}}}{1 - e^{-\frac{h\nu}{kT}}} + \frac{\left(\frac{h\nu}{kT}\right)^2}{2} \frac{1 + 3e^{-\frac{h\nu}{kT}}}{\left(1 - e^{-\frac{h\nu}{kT}}\right)^2} \right\} \right] \tag{5}$$

The fitting shows the Eq. 5 to the COBE/FIRAS data shown in Fig. 2.

2.2 Application of the BRI technique to find the mean temperature and spreading using the best-fit value of q

2.2.1 For Eq. 2 (q=0.99888)

Blackbody radiation refers to the electromagnetic radiation emitted by an idealised object known as a blackbody. A blackbody is an object that absorbs all incident radiation and emits radiation at all wavelengths according to its temperature. The spectral radiance of a blackbody is described by Planck’s law, which relates

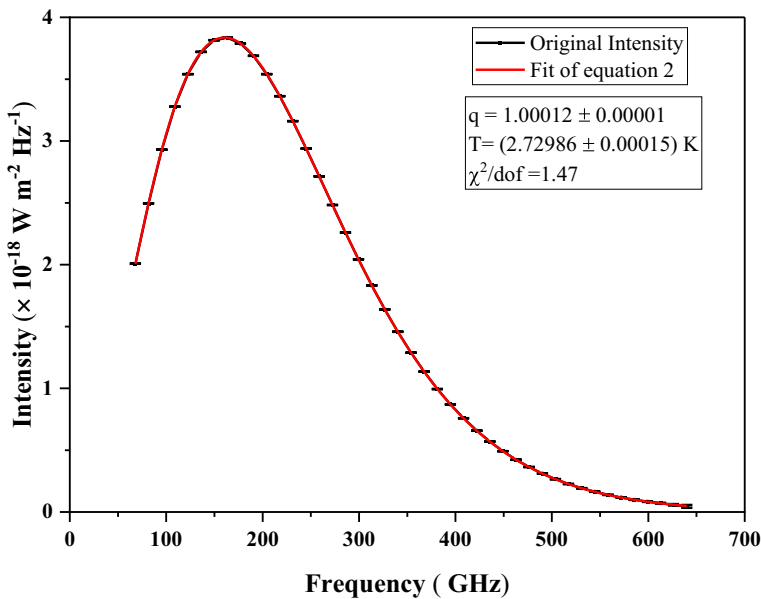


Fig. 2 Fitting of Eq. 5 with experimental data is shown. The value of $\chi^2/\text{dof}=60.27/41=1.47$ and the value of T shows a good fitting. The fitting value of q is found to be 1.00012 ± 0.00001

the temperature of the blackbody to the intensity of radiation emitted at different frequencies [30, 31]. Here, we have considered the generalised Planck's law, which includes q (i.e., entropy index different from unity). So, from Eq. 2, we can write a dimensionless parameter $G_1(\nu) = \frac{c^2}{2h\nu^3} I_1(\nu)$ as in Eq. 6 (for mathematical simplicity).

$$G_1(\nu) = \frac{e^{(2q-1)\frac{h\nu}{kT}} - e^{(q-1)\frac{h\nu}{kT}}}{\left\{ e^{(2q-1)\frac{h\nu}{kT}} - 1 \right\}^2} \quad (6)$$

Typically, telescopes are employed to measure the power spectrum of celestial objects. However, telescopes have a limited field of view, allowing them to observe only a tiny section of the sky at a given time. These observed sections consist of various blackbody radiators, each with temperature (T), all in thermal equilibrium. When considering a collection of blackbodies with a probability distribution, say $\alpha(T)$ (for different cases we have mentioned as $\alpha_1(T)$, $\alpha_2(T)$, $\alpha_3(T)$), the total power radiated per unit area can be determined by integrating over the temperature distribution as,

$$G_1(\nu) = \int_0^\infty \frac{e^{(2q-1)\frac{h\nu}{kT}} - e^{(q-1)\frac{h\nu}{kT}}}{\left\{ e^{(2q-1)\frac{h\nu}{kT}} - 1 \right\}^2} \alpha_1(T) dT \quad (7)$$

Equation (7) is a Fredholm integral equation known as an ill-posed problem. Ill-posedness refers to the instability of the result for tiny fluctuation in the input parameters. Historically, multiple methods have been employed to solve such integrals, which involve Laplace transform by Bojarski [32], Tikhonov regularisation method [33], universal function set method [34], Mellin transform set method [35], the modified Mobius inverse formula [36], maximum entropy method [37], regularised GMRES method [38] and Bernstein polynomials [39] among many. One common problem with these methods is the number of required data points for a stable inversion, which is 50 in the reference 32,36 and 37 in the reference. The literature presents one way to circumvent this requirement while producing a stable solution [40]. It assumes a probability distribution with unknown parameters, which can be calculated using the spectral data. The authors have shown how this approach can reproduce the input data robustly. The choice of the function is further modified in the paper [41], with a Gaussian distribution function resulting in tighter constraints of CMB spectral distortions. Although the initially chosen functions are different in these studies, the final functions converge to a Gaussian, which is to be expected, assuming the data are instances of a random distribution. In this research paper, a simple approach for blackbody radiation inversion, which relies on only three input data points, has been applied. Moreover, this method boasts a smaller program size compared to previous methods. Consequently, the current blackbody radiation inversion technique significantly reduces the overall program's complexity.

In Eq. 7, the total integral over space is taken. Referring to earlier experimental data [28], the cosmic microwave background (CMB) spectrum exhibits similarities to

that of a blackbody spectrum characterised by a temperature of (2.72548 ± 0.00057) K. The full width at a tenth of the maximum (FWTM) for a Gaussian distribution is $4.29193 z$ (z is the standard deviation). For a reasonable choice of $z=0.8$ and $T=2.72548$ K; $T_1= 2.72548 - \frac{1}{2} \times 0.8 \times 4.29193 = 1.008$ K and $T_2= 2.72548 + \frac{1}{2} \times 0.8 \times 4.29193 = 4.442$ K. So, it's reasonable to choose the limit from 1 K to 6 K for considering beyond $1z$. The limits in the integration correspond to the temperature distribution width for a tenth of maxima in the probability distribution. The contribution from the probability distribution function beyond these points is negligible and not considered. Furthermore, for clarification, we have checked the variation of results for different T_1 and T_2 in the later section.

$$So, G_1(\nu) = \int_{T_1}^{T_2} \frac{e^{\frac{(2q-1)h\nu}{kT}} - e^{\frac{(q-1)h\nu}{kT}}}{\left\{ e^{\frac{(2q-1)h\nu}{kT}} - 1 \right\}^2} \alpha_1(T) dT \tag{8}$$

To solve this Fredholm equation of the second kind, we need to employ a change of variable [39], $T=T_1 + (T_2 - T_1) t$. The newly introduced variable 't' falls within the range of values from 0 to 1. The value of 't' in terms of 'T' is $t = \frac{T-T_1}{T_2-T_1} = \frac{T-1}{5}$. The value of q used here is obtained from fitting (Fig. 1), i.e., 0.99888.

$$G_1(\nu) = (T_2 - T_1) \int_0^1 \frac{e^{\frac{(2q-1)h\nu}{k(T_1+(T_2-T_1)t)}} - e^{\frac{(q-1)h\nu}{k(T_1+(T_2-T_1)t)}}}{\left\{ e^{\frac{(2q-1)h\nu}{k(T_1+(T_2-T_1)t)}} - 1 \right\}^2} \alpha_1(T_1 + (T_2 - T_1) t) dt \tag{9}$$

We now assume an analytical Gaussian function $w(t) = \alpha (T_1 + (T_2 - T_1) t) = x.e^{-\left(\frac{(t-y)^2}{r^2}\right)}$. Here 'x' denotes the overall amplitude, 'y' represents the peak position of the Gaussian function and 'r' indicates the full width at half maximum. The chosen function $w(t)$ is used in the literature [41] and validated for standard extensive case ($q=1$). We will continue our work employing the identical function for non-extensive case. Employing $w(t)$ in Eq. (9) it becomes,

$$G_1(\nu) = (T_2 - T_1) \int_0^1 \frac{e^{\frac{(2q-1)h\nu}{k(T_1+(T_2-T_1)t)}} - e^{\frac{(q-1)h\nu}{k(T_1+(T_2-T_1)t)}}}{\left\{ e^{\frac{(2q-1)h\nu}{k(T_1+(T_2-T_1)t)}} - 1 \right\}^2} x.e^{-\left(\frac{(t-y)^2}{r^2}\right)} dt \tag{10}$$

Our objective is to determine the distribution $\alpha_1(T)$; therefore, the probability function is expressed in terms of 'T'. $w(t)$ can be rewritten in terms of 'T' as follows:

$$w(T) = x.e^{-\left(\frac{\left(\left(\frac{T-1}{5}\right)-y\right)^2}{r^2}\right)} \tag{11}$$

The experimental value of $G(\nu)$ can be calculated using Eq. 12 (for subsections 2. b. i, 2. b. ii, 2. b. iii, it will be $G_1(\nu)$, $G_2(\nu)$, $G_3(\nu)$, respectively). The experimental values of $I_{monopole}$ are given [24].

$$G(\nu) = \frac{c^2}{2h\nu^3} I_{monopole} \tag{12}$$

Taking Eq. (10) into the left-hand side and using the calculated $G_1(\nu)$ from Eq. (12) on the right-hand side, a set of three equations is derived for a corresponding set of three frequencies. These equations are then mathematically simulated, determining x , y , and r values. This process is repeated for another nine sets of frequencies, and the obtained values are organised in a table. The calculated x , y , and r values are plugged into Eq. (11), leading to the generation of ten probability distributions (pdf) of temperature (for each set of frequencies). We have used more data sets (10 sets), ensuring comprehensive coverage over the entire frequency spectrum. All the calculated parameters are listed in Table 1.

$$Y(T) = \frac{\sum a_i(T)}{10} \tag{13}$$

$Y(T)$ is the average of all probability distribution functions. Figure 3 below shows a plot of $Y(T)$ against temperature.

2.2.2 For Eq. 5 { $q = 1.00012$ (Tsallis Formula)}

We delve deeper into a more coherent scenario by examining a non-extensive formulation of Planck’s distribution, as expressed by Eq. 5. Here, we will apply the BRI technique to find the probability distribution function of temperature. The q value used for calculation is found from fitting in Fig. 2, i.e., $q = 1.00012$.

Equation 5 can be written in terms of dimensionless parameter $G_2(\nu) = \frac{c^2}{2h\nu^3} I_2(\nu)$

Table 1 The values of x , y , r for different probability functions, each denoted by symbols as $a_1(T), a_2(T), a_3(T), a_4(T), a_5(T), a_6(T), a_7(T), a_8(T), a_9(T), a_{10}(T)$ is given. Each corresponds to distinct frequency sets

Frequency set ($\times 10^{11}$ Hz)	x	y	r	Probability functions
0.681, 0.954, 1.224	24.99157176320	0.34738924807	0.00462286012	$a_1(T)$
1.498, 1.770, 2.043	15.23300327964	0.34693340406	0.00731052671	$a_2(T)$
2.724, 2.994, 3.267	26.03309678746	0.34461718492	0.00432923691	$a_3(T)$
2.859, 3.132, 3.402	24.00511550630	0.34346319362	0.00474877201	$a_4(T)$
3.267, 3.541, 3.813	26.99877540257	0.34610077415	0.00410711582	$a_5(T)$
3.948, 4.221, 4.491	25.25503759636	0.34408459373	0.00449263429	$a_6(T)$
4.083, 4.356, 4.629	15.57654569695	0.34402593580	0.00727679172	$a_7(T)$
2.724, 3.132, 3.540	23.68563488528	0.34440869672	0.00476703159	$a_8(T)$
4.083, 4.491, 4.902	24.14713525522	0.34528641888	0.00461536951	$a_9(T)$
5.445, 5.583, 6.261	21.57305875014	0.34192473913	0.00548357002	$a_{10}(T)$

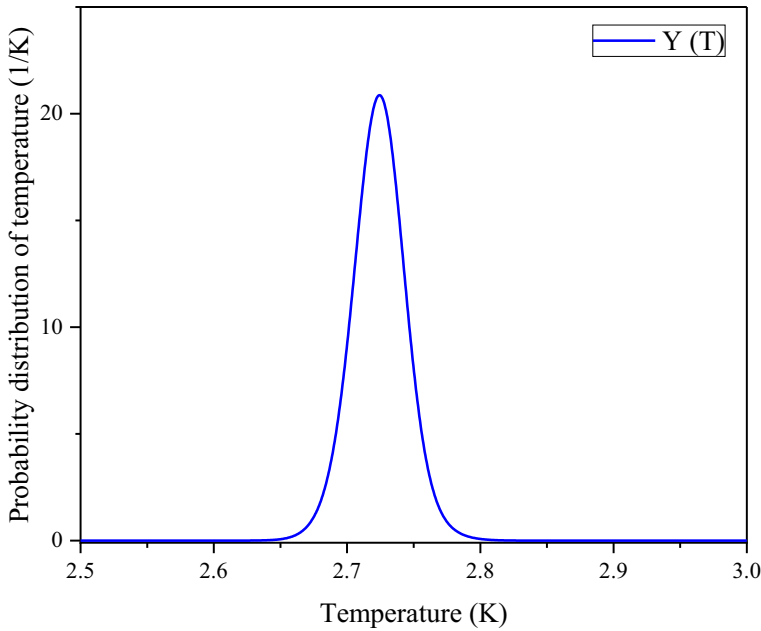


Fig. 3 $Y(T)$ versus temperature is shown. To enhance the clarity of the graph, the x-axis scale is taken from 2.5 K to 3.0 K

$$G_2(\nu) = \frac{1}{e^{\frac{h\nu}{kT}} - 1} \left[1 + (q - 1) \left\{ \ln \left(1 - e^{-\frac{h\nu}{kT}} \right) - \frac{h\nu}{kT} \frac{1 + e^{-\frac{h\nu}{kT}}}{1 - e^{-\frac{h\nu}{kT}}} + \frac{\left(\frac{h\nu}{kT} \right)^2}{2} \frac{1 + 3e^{-\frac{h\nu}{kT}}}{\left(1 - e^{-\frac{h\nu}{kT}} \right)^2} \right\} \right] \tag{14}$$

The same Blackbody Radiation Inversion (BRI) technique and methodology mentioned in subsection 2.b.i is utilised in this subsection. Hence, from Eq. 5, it is possible to compute a dimensionless parameter, $G_2(\nu)$. This is to reduce the mathematical complexity. Additionally, by introducing $\alpha_2(T)$ as the chosen probability distribution function (pdf) and integrating over the temperature range from $T_1 = 1$ K to $T_2 = 6$ K, along with employing a change in a variable, Eq. 14 can be expressed as follows.

$$G_2(\nu) = (T_2 - T_1) \int_0^1 \frac{1}{e^{\frac{h\nu}{k(T_1 + (T_2 - T_1)t)}} - 1} \left[1 + \left\{ \ln \left(1 - e^{-\frac{h\nu}{k(T_1 + (T_2 - T_1)t)}} \right) - \frac{h\nu}{k(T_1 + (T_2 - T_1)t)} \frac{1 + e^{-\frac{h\nu}{k(T_1 + (T_2 - T_1)t)}}}{1 - e^{-\frac{h\nu}{k(T_1 + (T_2 - T_1)t)}}} + \frac{\left(\frac{h\nu}{k(T_1 + (T_2 - T_1)t)} \right)^2}{2} \frac{1 + 3e^{-\frac{h\nu}{k(T_1 + (T_2 - T_1)t)}}}{\left(1 - e^{-\frac{h\nu}{k(T_1 + (T_2 - T_1)t)}} \right)^2} \right\} \right] \alpha_2(T_1 + (T_2 - T_1)t) dt \tag{15}$$

Now, introducing our chosen Gaussian function $w(t)$ in the place of $\alpha_2(T_1 + (T_2 - T_1)t)$, we can find the value of pdf. By substituting Eq. (15) into the L.H.S. and using the calculated $G(\nu)$ from Eq. (12) R.H.S., a set of three equations is derived for a corresponding set of three frequencies. These equations are then computed, and the values for x , y , and r , are determined. This process is repeated for another nine sets of frequencies, and the obtained values are listed in Table 2. For each set of frequencies, the calculated x , y , and r values are plugged into Eq. (11), leading to the generation of ten probability distributions of temperature.

$$B(T) = \frac{\sum b_i(T)}{10} \tag{16}$$

$B(T)$ is the average of all probability distribution functions. The following Fig. 4 illustrates the average function $B(T)$ against temperature.

2.2.3 Putting $q = 1$ in Eq. 1 or 2

In the preceding Sect. (2.2.1 and 2.2.2), we employ the methodology of blackbody radiation inversion to find the average probability distribution of temperature. Now, in this section, we aim to evaluate the find the average probability distribution of temperature through the approach of extensive statistics. We set the parameter q equal to 1 in Eq. 1 or 2 to achieve this. When we substitute this value into either Eq. 1 or 2, the expressions take the following form:

$$I_3(\nu) = \frac{2h\nu^3}{c^2} \frac{1}{\left(e^{\frac{h\nu}{kT}} - 1\right)} \tag{17}$$

Table 2 Values and notations for various probability functions, which correspond to multiple sets of frequencies, are given

Frequency set ($\times 10^{11}$ Hz)	x	y	r	Probability functions
0.681, 0.954, 1.224	23.18688369665	0.34831318680	0.00498432210	$b_1(T)$
1.498, 1.770, 2.043	13.97468472571	0.34793445573	0.00796729670	$b_2(T)$
2.724, 2.994, 3.267	28.42686300703	0.34557635352	0.00396649055	$b_3(T)$
2.859, 3.132, 3.402	25.76065425021	0.34440705130	0.00442766977	$b_4(T)$
3.267, 3.541, 3.813	29.35443074676	0.34700872027	0.00381229927	$b_5(T)$
3.948, 4.221, 4.491	15.78327681037	0.34420208450	0.00721293741	$b_6(T)$
4.083, 4.356, 4.629	15.49667682580	0.34482300680	0.00733053579	$b_7(T)$
2.724, 3.132, 3.540	25.10176834217	0.34535899761	0.00450042289	$b_8(T)$
4.083, 4.491, 4.902	22.41867547118	0.34606165659	0.00498336435	$b_9(T)$
5.445, 5.583, 6.261	12.47900083833	0.34328579201	0.00935229646	$b_{10}(T)$

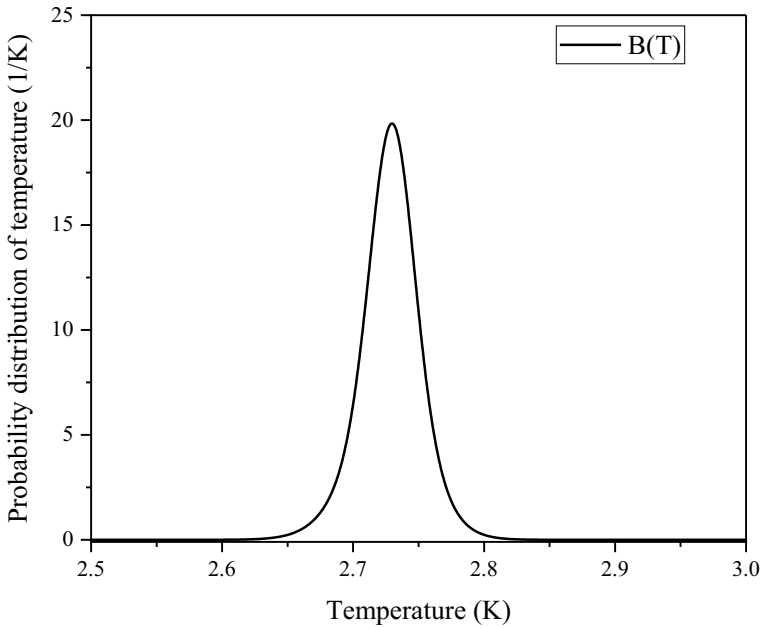


Fig. 4 $B(T)$ versus temperature is shown. To enhance the clarity of the graph, the x-axis scale is taken from 2.5 K to 3.0 K

Applying the BRI approach (Mentioned in detail in Sect. 2.2.1 and 2.2.2) we get the integral equation as,

$$G_3(\nu) = (T_2 - T_1) \int_0^1 \frac{\alpha_3(T_1 + (T_2 - T_1)t)}{\left(e^{\frac{h\nu}{k(T_1+(T_2-T_1)t)}} - 1 \right)} dt \tag{18}$$

In this approach, the defined Gaussian function denoted as $w(t) = \alpha (T_1 + (T_2 - T_1) t) = x \cdot e^{-\left(\frac{(t-y)^2}{r^2}\right)}$ is substituted for α_3 in Eq. 18. It becomes,

$$G_3(\nu) = (T_2 - T_1) \int_0^1 \frac{x \cdot e^{-\left(\frac{(t-y)^2}{r^2}\right)}}{\left(e^{\frac{h\nu}{k(T_1+(T_2-T_1)t)}} - 1 \right)} dt \tag{19}$$

This helps determine the probability distribution function. By plugging this substitution into Eq. 19 and equating it to a precomputed value of $G(\nu) = \frac{c^2}{2h\nu^3} I_{monopole}$ in Eq. 12, a set of three equations is derived for three frequencies. These equations are then solved through mathematical simulation to find values for parameters x , y , and r . The same process is repeated for another nine sets of three frequencies. Using these values, ten temperature probability distributions are generated using Eq. 11. All the values of x , y , and r , and the notation of pdfs are listed in Table 3.

The average of the above probability distributions is denoted as $X(T)$.

Table 3 Values of x , y , r and notations for various probability functions are given. Each corresponds to a distinct set of frequencies

Frequency set ($\times 10^{11}$ Hz)	x	y	r	Probability functions
0.681, 0.954, 1.224	23.08751182288	0.34839798523	0.00500455015	$c_1(T)$
1.498, 1.770, 2.043	35.35498162270	0.34820092725	0.00314753401	$c_2(T)$
2.724, 2.994, 3.267	28.96838330599	0.34583664143	0.00388667268	$c_3(T)$
2.859, 3.132, 3.402	25.74534855035	0.34468155091	0.00442335935	$c_4(T)$
3.267, 3.541, 3.813	30.36538651935	0.34733558723	0.00364765037	$c_5(T)$
3.948, 4.221, 4.491	27.65257154203	0.34532293251	0.00409808079	$c_6(T)$
4.083, 4.356, 4.629	14.08039209747	0.34517696598	0.00804558056	$c_7(T)$
2.724, 3.132, 3.540	27.84837070320	0.34563978703	0.00405011100	$c_8(T)$
4.083, 4.491, 4.902	22.32301608506	0.34648764970	0.00498792263	$c_9(T)$
5.445, 5.583, 6.261	12.45815410715	0.34379063057	0.00932532516	$c_{10}(T)$

$$X(T) = \frac{\sum c_i(T)}{10} \quad (20)$$

The following Fig. 5 illustrates the average ten distinct probability functions.

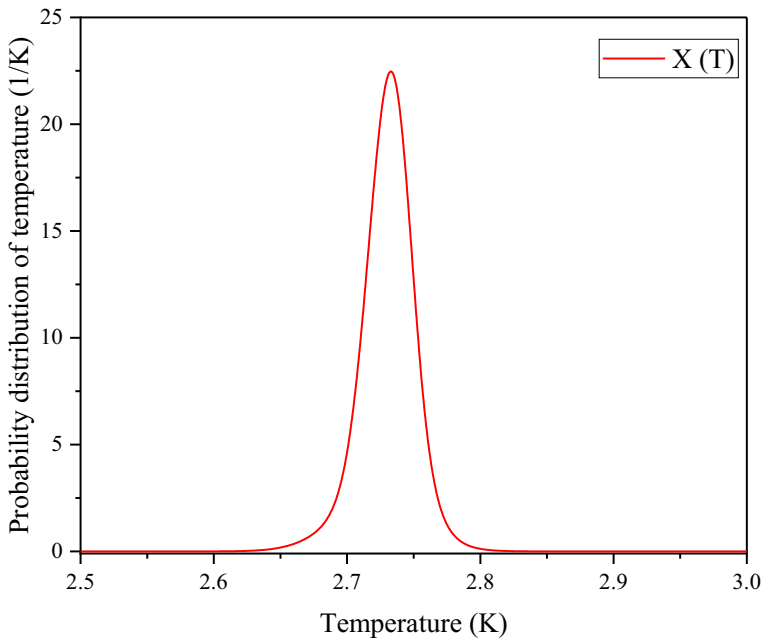


Fig. 5 $X(T)$ vs. temperature is shown. To enhance the clarity of the graph, the x-axis scale is taken from 2.5 K to 3.0 K

3 Results

3.1 For Sect. 2.2.1

The Normalised probability distribution of temperature is given by,

$$\alpha_1(T) = \frac{1}{\int_1^6 Y(T)dT} \times Y(T) = 0.995 \times Y(T) \tag{21}$$

The ‘mean normalised temperature’ and ‘spreading’ is given by.

$$T = \int_1^6 T.\alpha_1(T)dT \cong 2.723K \tag{22}$$

$$\alpha^2 = \int_1^6 (T - 2.723)^2 \alpha_1(T)dT = 1.412 \times 10^{-4} \tag{23}$$

Interpreting the spreading as uncertainty, the value of σ is calculated to be 0.012 K.

We used the calculated normalised $\alpha_1(T)=0.995 \times Y(T)$ and $T=2.723$ K in the following Eq. 24 to reconstruct the radiation intensity. This is to access the accuracy of our approach of solving BRI problem. Figure 6 compares the original spectrum data from COBE/FIRAS and the reconstructed data.

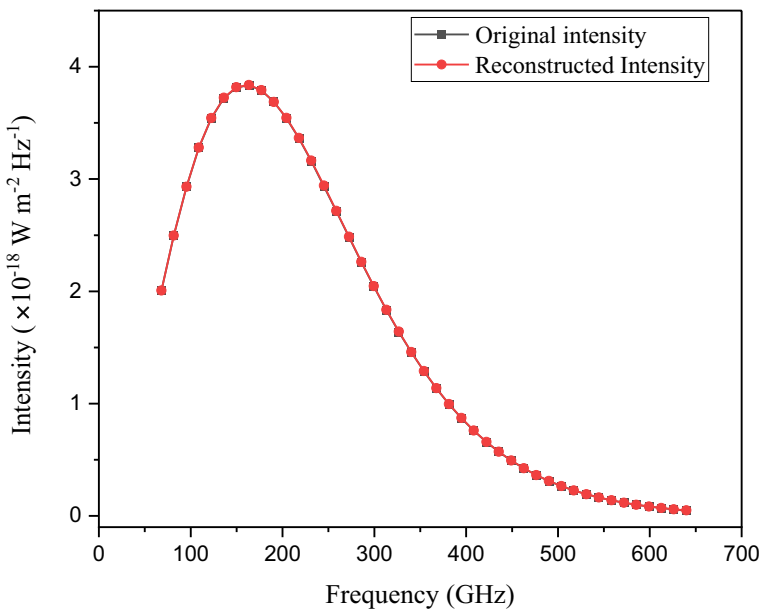


Fig. 6 Illustrates the experimental and reconstructed intensities graphed against frequency. It demonstrates a significant similarity between the reconstructed and COBE/FIRAS datasets

$$I_1(\nu) = \frac{2h\nu^3}{c^2} \int_1^6 \frac{e^{(2q-1)\frac{h\nu}{kT}} - e^{(q-1)\frac{h\nu}{kT}}}{\left\{ e^{(2q-1)\frac{h\nu}{kT}} - 1 \right\}^2} \times 0.995 \times Y(T)dT \tag{24}$$

The frequencies, along with the corresponding original and reconstructed intensities with corresponding uncertainties relevant to the above figure are enumerated in a table (refer Appendix 1).

$$\chi^2 = \sum w_i [(R_i - O_i)]^2 \tag{25}$$

Equation 25, represented by χ^2 , is the sum of weighted squared differences between the reconstructed data points (R_i) and the original data points (O_i). The weights (w_i) are determined by $\frac{1}{\sigma_i^2}$ on each data point.

The values of σ_i , denoting the errors/uncertainties in the data points, can be found in the referenced paper [11]. The reduced chi-square (χ^2/dof), where dof represents the number of degrees of freedom, has been calculated to be 1.07 (calculated using data given in Appendix 1). Here the number of degrees of freedom is 43.

3.2 For Sect. 2.2.2

The Normalised probability distribution of temperature is denoted as $\alpha_2(T)$.

$$\alpha_2(T) \frac{1}{\int_1^6 B(T)dT} \times B(T) = 0.995 \times B(T) \tag{26}$$

The ‘first order moment’ or the ‘mean normalised temperature’ and second order moment’ or ‘spreading’ is calculated as

$$T = \int_1^6 T \cdot \alpha_2(T)dT \cong 2.727K \tag{27}$$

$$\alpha^2 = 0.995 \int_1^6 (T - 2.726)^2 \alpha_2(T)dT = 3.691 \times 10^{-4} \tag{28}$$

Hence, σ (spreading in pdf of temperature)=0.019 K.

By utilising the calculated $\alpha_2(T)=0.995 \times B(T)$ and $T=2.727$ K in the following Eq. 29, we reconstructed the radiation intensity. Figure 7 compares the original spectrum data from COBE/FIRAS and the reconstructed data.

$$I_2(\nu) = \frac{2h\nu^3}{c^2} \int_1^6 \frac{1}{e^{\frac{h\nu}{kT}} - 1} \left[1 + \left\{ \ln \left(1 - e^{-\frac{h\nu}{kT}} \right) - \frac{h\nu}{kT} \frac{1 + e^{-\frac{h\nu}{kT}}}{1 - e^{-\frac{h\nu}{kT}}} + \frac{\left(\frac{h\nu}{kT}\right)^2}{2} \frac{1 + 3e^{-\frac{h\nu}{kT}}}{\left(1 - e^{-\frac{h\nu}{kT}}\right)^2} \right\} \right] \times 0.995 \times B(T)dT \tag{29}$$

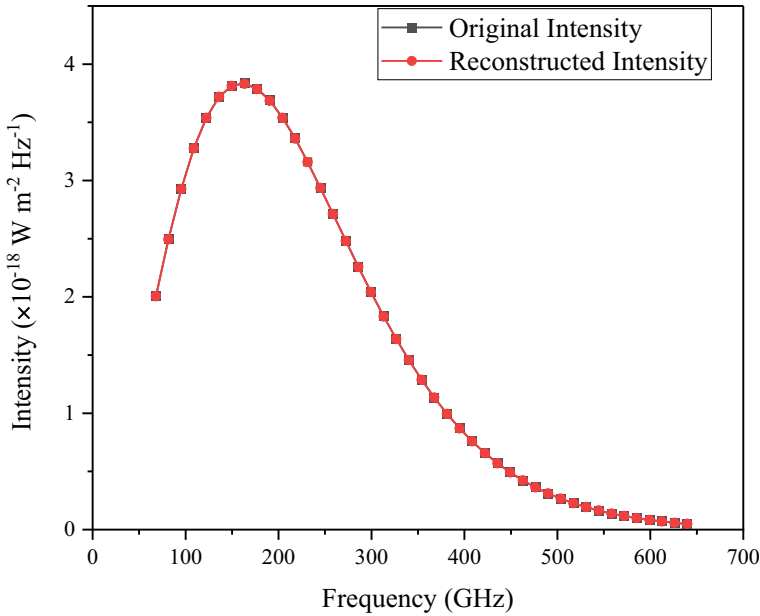


Fig. 7 Illustrates the experimental and reconstructed intensities (using Eq. 29) graphed against frequency. It demonstrates a significant similarity between the reconstructed and COBE/FIRAS datasets

Refer Appendix 2 for all the relevant data produced for Fig. 7. The reduced chi-square using Eq. 25 is calculated to be 1.07.

3.3 For Sect. 2.2.3

The normalised probability distribution of temperature is denoted as $\alpha_3(T)$.

$$\alpha_3(T) \frac{1}{\int_1^6 X(T) dT} \times X(T) = 0.998 \times X(T) \tag{30}$$

The ‘first order moment’ or the ‘mean normalised temperature’ and ‘second order moment’ or ‘spreading’ is calculated as.

$$T = \int_1^6 T \cdot \alpha_3(T) dT \cong 2.732K \tag{31}$$

$$\alpha^2 \int_1^6 (T - 2.732)^2 \alpha_3(T) dT = 1.844 \times 10^{-4} \tag{32}$$

From this, the uncertainty in temperature $\sigma = 0.014$ K.

By utilising the calculated $\alpha_3(T) = 0.998 \times X(T)$ and $T = 2.732$ K in the following Eq. 33, we reconstructed the radiation intensity. Figure 8 compares the original spectrum data from COBE/FIRAS and the reconstructed data.

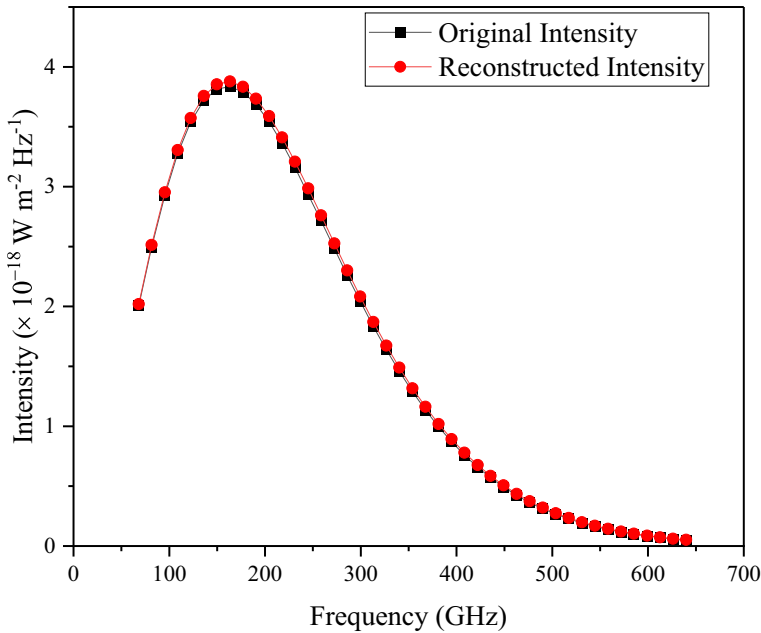


Fig. 8 Illustrates the experimental and reconstructed intensities graphed against frequency. It demonstrates a significant similarity between the reconstructed and COBE/FIRAS datasets. The reduced chi-square is calculated to be 1.07 using Eq. 25

$$I_3(\nu) = \frac{2h\nu^3}{c^2} \int_1^6 \frac{0.998 \times X(T)}{\left(e^{\frac{h\nu}{kT}} - 1 \right)} dT \tag{33}$$

All the relevant data for Fig. 8 is listed in Appendix 3.

The calculation of temperature and spreading for CMB monopole spectrum (using $q=1$, i.e., standard Planck’s law) was done in the literature [40]. In that paper, the author used four distinct probability functions. Here, we have increased the number of probability functions, i.e., ten functions. Importantly, we have maintained consistent frequencies across all three cases (in Sect. 2.2.1, 2.2.2, and 2.2.3). This choice allows us to showcase the change in CMB temperature and its associated uncertainty. Furthermore, it’s noteworthy to mention that the results in reference [41] ($T=2.741 \pm 0.018$) K and in this work (2.732 ± 0.014) K are nearly consistent. Increasing the number of probability functions contributes to aligning the calculated temperature closer to the standard temperature, 2.72548 K.

We also incorporate experimental errors in Intensities ($\Delta I_{\text{monopole}}$) associated with these selected frequencies in Eq. 12 while calculating the temperature and its corresponding uncertainty. The values of errors (1σ) in intensity are given in NASA website [24] (also can refer appendices). Also, we can check the dependency of the result by varying the values of T_1 and T_2 within the range. All the values are listed below in Table 4.

Table 4 Variation in mean temperature and spreading with changing values of T_1 and T_2

Variation in result by change in temperature			
T_1 (K)	T_2 (K)	T (K)	σ or ΔT (K)
1.2	5.8	2.729	0.024
1.4	5.6	2.726	0.022
1.6	5.4	2.720	0.015
1.8	5.2	2.721	0.017
2	5	2.727	0.032
1	6	2.732	0.014
Variation in result by incorporating ΔI			
T (K)	σ or ΔT (K)		
2.730	0.014		

The above table shows that if we vary the integral limits within the chosen range, the value of mean temperature and spreading do not change much. All the values are nearly equal. So, taking integral value from 1 K to 6 K is reasonable.

4 Comparison of the probability distribution of temperatures $q = 1$, $q = 0.99888 \pm 00016$, $q = 1.00012 \pm 00001$

In the preceding sections, we have calculated the probability distribution of temperature for three different models described by Eqs. (2), (5), and (17). Equations 2 and 5 characterise a blackbody spectrum with non-extensive statistics, and Eq. 17 characterises a blackbody spectrum with extensive thermostatics. The existence of a non-extensive nature in the CMB spectra has been concluded [42] with $q = 1.045 \pm 0.005$ using Wilkinson Microwave Anisotropy Probe (WMAP) data at 99% confidence level. Our study incorporates values of $q = 0.99888 \pm 00016$ ($|q - 1| = 10^{-3}$), $q = 1.00012 \pm 00001$ ($|q - 1| = 10^{-4}$), and $q = 1$ at 95% confidence level. A comparison among the corresponding probability distribution functions is shown in Fig. 9. The vertical axis is the normalised probability distribution with units of $[\frac{1}{K}]$ while the horizontal axis is the temperature with units [K].

The figure illustrates that the mean value of all probability distributions is nearly the same. We have summarised our findings in Table 5.

The best-fit value of $q \approx 1$. This suggests that the system exhibits behaviour close to extensivity. The uncertainties associated with the q values are very small, indicating a high level of confidence in the obtained results.

5 Discussion

Assuming that the CMB follows a perfect blackbody spectrum, the best-fit value of the temperature is observed as $T = 2.725$ K. Still, fluctuations $\frac{\Delta I}{I}$ of the order of 10^{-5} indicates presence of μ and y distortions, whose values can be estimated

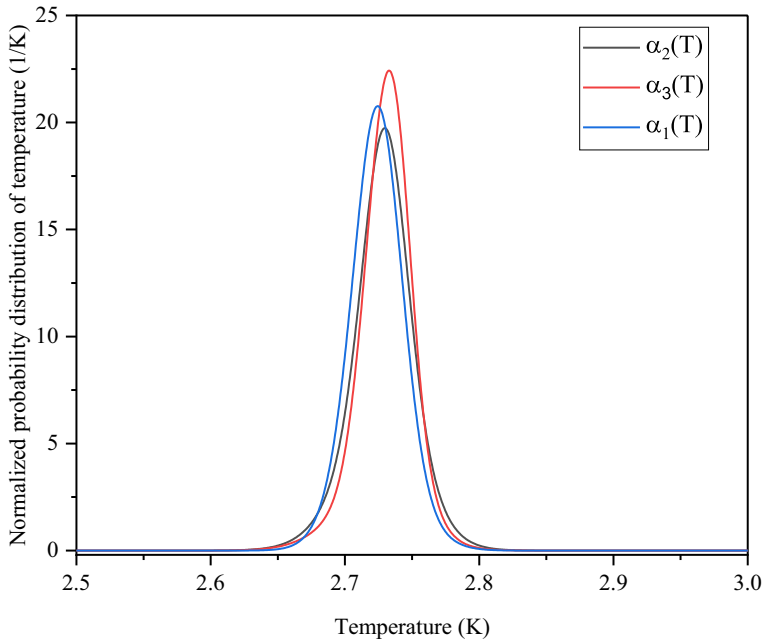


Fig. 9 Normalized probability distributions of temperature for $q=1$, $q=0.99888$ and $q=1.00012$ are shown. As the distributions are normalised, the relative height of the peaks denotes the relative probability, which is highest for $q=1$

Table 5 Summarized results of all the sections

q	1	0.99888 ± 0.00016	1.00012 ± 0.00001
$T \pm \Delta T(K)$	2.732 ± 0.014	2.723 ± 0.012	2.727 ± 0.019

using the COBE data and the lower/upper bounds are $\mu < 10^{-5}$ and $y < 10^{-6}$ respectively according to fixsen et al. [11]. Mixing of blackbodies also leads to μ and y distortions and can be estimated by the formula $\mu = 2.8 \times \left(\frac{\Delta T}{T}\right)^2$ and $y = 0.5 \times \left(\frac{\Delta T}{T}\right)^2$ [43]. Here, for $q=1$, $\frac{\Delta T}{T}$ is 0.0051. Hence $\mu = 7.2 \times 10^{-5}$ and $y = 1.3 \times 10^{-5}$; which are close to the values as explained by fixsen et al. We calculate $|q - 1| = 10^{-3}$ and $|q - 1| = 10^{-4}$ for two cases by fitting COBE/FIRAS data with Eqs. 2 and 5, indicating departures from the extensive Planck blackbody law. While no formula for μ and y distortions using non-extensive Planck blackbodies in the literature, our analysis suggests that their values would be similar to those in the extensive case due to the similarity in $\frac{\Delta T}{T}$. The value of $\frac{\Delta T}{T}$ ($= 0.0044$ for $q < 1$) and ($= 0.00696$ for $q > 1$) are close to the extensive case and μ and y depends on $\frac{\Delta T}{T}$. Therefore, the upper limits of μ and y from this study are expected to be approximately the same as in the extensive and Fixsen cases.

Appendix 1

All the original intensities and reconstructed intensities along with their uncertainties relevant to Fig. 6 are listed below.

Frequency (GHz)	Intensity ($\times 10^{-18} \text{ W m}^{-2} \text{ Hz}^{-1}$)	Uncertainties ($\times 10^{-22} \text{ W m}^{-2} \text{ Hz}^{-1}$)	Intensity ($\times 10^{-18} \text{ W m}^{-2} \text{ Hz}^{-1}$)	Uncertainties ($\times 10^{-20} \text{ W m}^{-2} \text{ Hz}^{-1}$)
	Original		Reconstructed	
68.1	2.007	1.4	2.008	3.0
81.6	2.495	1.9	2.497	4.1
95.4	2.930	2.5	2.932	5.3
108.9	3.277	2.3	3.280	6.5
122.4	3.540	2.2	3.543	7.6
136.2	3.720	2.1	3.724	8.7
149.7	3.814	1.8	3.818	9.6
163.5	3.834	1.8	3.838	10.3
177.0	3.789	1.6	3.792	10.9
190.5	3.688	1.4	3.687	11.3
204.3	3.540	1.3	3.544	11.5
217.8	3.362	1.2	3.366	11.7
231.3	3.160	1.1	3.164	11.6
245.1	2.932	1.0	2.942	11.4
258.6	2.714	1.1	2.717	11.0
272.4	2.482	1.2	2.486	10.5
285.9	2.259	1.4	2.262	10.1
299.4	2.043	1.6	2.046	9.6
313.2	1.832	1.8	1.835	8.9
326.7	1.638	2.2	1.641	8.3
340.2	1.457	2.2	1.460	7.7
354.0	1.288	2.3	1.290	7.1
367.5	1.135	2.3	1.138	6.4
381.3	0.994	2.3	0.996	5.9
394.8	0.870	2.2	0.872	5.3
408.3	0.758	2.1	0.760	4.8
422.1	0.657	2.0	0.659	4.3
435.6	0.570	1.9	0.571	3.9
449.1	0.492	1.9	0.493	4.0
462.9	0.422	1.9	0.424	3.1
476.4	0.363	2.1	0.364	2.7
490.2	0.310	2.3	0.311	2.4
503.7	0.265	2.6	0.266	2.1
517.2	0.226	2.8	0.227	1.8
531.0	0.192	3.0	0.193	1.6
544.5	0.163	3.2	0.164	1.4

Frequency (GHz)	Intensity ($\times 10^{-18} \text{ W m}^{-2} \text{ Hz}^{-1}$)	Uncertainties ($\times 10^{-22} \text{ W m}^{-2} \text{ Hz}^{-1}$)	Intensity ($\times 10^{-18} \text{ W m}^{-2} \text{ Hz}^{-1}$)	Uncertainties ($\times 10^{-20} \text{ W m}^{-2} \text{ Hz}^{-1}$)
	Original		Reconstructed	
558.3	0.138	3.3	0.139	1.2
571.8	0.117	3.5	0.118	1.1
585.3	0.099	4.1	0.099	0.9
599.1	0.083	5.5	0.084	0.7
612.6	0.070	8.8	0.071	0.7
626.1	0.058	15.5	0.059	0.6
639.9	0.045	28.2	0.050	0.5

Appendix 2

All the original intensities and reconstructed intensities along with their uncertainties relevant to Fig. 7 are listed below.

Frequency (GHz)	Intensity ($\times 10^{-18} \text{ W m}^{-2} \text{ Hz}^{-1}$)	Uncertainties ($\times 10^{-22} \text{ W m}^{-2} \text{ Hz}^{-1}$)	Intensity ($\times 10^{-18} \text{ W m}^{-2} \text{ Hz}^{-1}$)	Uncertainties ($\times 10^{-20} \text{ W m}^{-2} \text{ Hz}^{-1}$)
	Original		Reconstructed	
68.1	2.007	1.4	2.006	4.8
81.6	2.495	1.9	2.494	6.6
95.4	2.930	2.5	2.928	8.5
108.9	3.277	2.3	3.276	10.3
122.4	3.540	2.2	3.538	12.0
136.2	3.720	2.1	3.719	13.7
149.7	3.814	1.8	3.812	15.1
163.5	3.834	1.8	3.832	16.3
177.0	3.789	1.6	3.786	17.2
190.5	3.688	1.4	3.685	17.9
204.3	3.540	1.3	3.538	18.2
217.8	3.362	1.2	3.36	18.4
231.3	3.160	1.1	3.158	18.1
245.1	2.932	1.0	2.936	17.9
258.6	2.714	1.1	2.712	17.4
272.4	2.482	1.2	2.480	16.8
285.9	2.259	1.4	2.257	16.0
299.4	2.043	1.6	2.041	15.1
313.2	1.832	1.8	1.831	14.1
326.7	1.638	2.2	1.637	13.1
340.2	1.457	2.2	1.457	12.2
354.0	1.288	2.3	1.287	11.5

Frequency (GHz)	Intensity ($\times 10^{-18} \text{ W m}^{-2} \text{ Hz}^{-1}$)	Uncertainties ($\times 10^{-22} \text{ W m}^{-2} \text{ Hz}^{-1}$)	Intensity ($\times 10^{-18} \text{ W m}^{-2} \text{ Hz}^{-1}$)	Uncertainties ($\times 10^{-20} \text{ W m}^{-2} \text{ Hz}^{-1}$)
	Original		Reconstructed	
367.5	1.135	2.3	1.135	10.3
381.3	0.994	2.3	0.994	9.5
394.8	0.870	2.2	0.870	8.4
408.3	0.758	2.1	0.759	7.6
422.1	0.657	2.0	0.657	6.9
435.6	0.570	1.9	0.570	6.1
449.1	0.492	1.9	0.492	5.4
462.9	0.422	1.9	0.423	4.8
476.4	0.363	2.1	0.363	4.2
490.2	0.310	2.3	0.311	3.7
503.7	0.265	2.6	0.266	3.3
517.2	0.226	2.8	0.227	2.9
531.0	0.192	3.0	0.193	2.6
544.5	0.163	3.2	0.164	2.2
558.3	0.138	3.3	0.138	1.9
571.8	0.117	3.5	0.117	1.7
585.3	0.099	4.1	0.099	1.4
599.1	0.083	5.5	0.083	1.2
612.6	0.070	8.8	0.070	1.1
626.1	0.058	15.5	0.059	0.9
639.9	0.045	28.2	0.050	0.8

Appendix 3

All the original intensities and reconstructed intensities along with their uncertainties relevant to Fig. 8 are listed below.

Frequency (GHz)	Intensity ($\times 10^{-18} \text{ W m}^{-2} \text{ Hz}^{-1}$)	Uncertainties ($\times 10^{-22} \text{ W m}^{-2} \text{ Hz}^{-1}$)	Intensity ($\times 10^{-18} \text{ W m}^{-2} \text{ Hz}^{-1}$)	Uncertainties ($\times 10^{-20} \text{ W m}^{-2} \text{ Hz}^{-1}$)
	Original		Reconstructed	
68.1	2.007	1.4	2.020	3.6
81.6	2.495	1.9	2.513	4.8
95.4	2.930	2.5	2.953	6.3
108.9	3.277	2.3	3.305	7.6
122.4	3.540	2.2	3.573	9.0
136.2	3.720	2.1	3.758	10.2
149.7	3.814	1.8	3.855	11.2
163.5	3.834	1.8	3.878	12.1

Frequency (GHz)	Intensity ($\times 10^{-18} \text{ W m}^{-2} \text{ Hz}^{-1}$)	Uncertainties ($\times 10^{-22} \text{ W m}^{-2} \text{ Hz}^{-1}$)	Intensity ($\times 10^{-18} \text{ W m}^{-2} \text{ Hz}^{-1}$)	Uncertainties ($\times 10^{-20} \text{ W m}^{-2} \text{ Hz}^{-1}$)
	Original		Reconstructed	
177.0	3.789	1.6	3.834	12.9
190.5	3.688	1.4	3.735	13.3
204.3	3.540	1.3	3.589	13.6
217.8	3.362	1.2	3.411	13.7
231.3	3.160	1.1	3.209	13.6
245.1	2.932	1.0	2.986	13.4
258.6	2.714	1.1	2.760	12.8
272.4	2.482	1.2	2.526	12.3
285.9	2.259	1.4	2.301	11.8
299.4	2.043	1.6	2.083	11.2
313.2	1.832	1.8	1.870	10.4
326.7	1.638	2.2	1.673	9.8
340.2	1.457	2.2	1.490	9.0
354.0	1.288	2.3	1.317	8.3
367.5	1.135	2.3	1.163	7.6
381.3	0.994	2.3	1.019	6.9
394.8	0.870	2.2	0.892	6.2
408.3	0.758	2.1	0.779	5.6
422.1	0.657	2.0	0.675	5.1
435.6	0.570	1.9	0.585	4.6
449.1	0.492	1.9	0.506	4.1
462.9	0.422	1.9	0.435	3.5
476.4	0.363	2.1	0.374	3.1
490.2	0.310	2.3	0.320	2.8
503.7	0.265	2.6	0.274	2.5
517.2	0.226	2.8	0.234	2.2
531.0	0.192	3.0	0.199	1.9
544.5	0.163	3.2	0.169	1.6
558.3	0.138	3.3	0.143	1.4
571.8	0.117	3.5	0.121	1.2
585.3	0.099	4.1	0.102	1.1
599.1	0.083	5.5	0.086	0.9
612.6	0.070	8.8	0.073	0.7
626.1	0.058	15.5	0.061	0.7
639.9	0.045	28.2	0.051	0.5

Acknowledgements The authors are grateful to the Department of Physics, Birla Institute of Technology, Mesra, Ranchi, for allotting an excellent research environment during the research work. The authors thank Koustav Konar and Soumen Karmakar for their help and support. The authors would also like to thank Balendu Pathak for encouraging this research. S. Dhal thanks UGC (Savitribai Jyotirao Phule Single Girl Child with grant number - UGCES-22-GE-ORI-F-SJSGC-3962) for the fellowship to carry out research.

Author contributions S. D. has performed the analysis, figure, and computational work and wrote the manuscript with text and figure. R. K. P. conceived the idea, wrote the manuscript, analysed and supervised the overall work for the final manuscript.

Data availability No datasets were generated or analysed during the current study.

Declarations

Competing interests The authors declare no competing interests.

References

1. Penzias, A.A., Wilson, R.W.: A measurement of excess antenna temperature at 4080 Mc/s. *Astrophys. J.* **142**, 419–421 (1965). <https://doi.org/10.1086/148307>
2. Peebles, P.J.E., Wilkinson, D.T.: The primeval fireball. *Sci. Am.* **216**(6), 28–37 (1967). <http://www.jstor.org/stable/24926025>
3. Dautcourt, G., Wallis, G.: The cosmic Blackbody radiation. *Fortschr. Phys.* **16**(10), 545–593 (1968). <https://doi.org/10.1002/prop.19680161002>
4. Partridge, R.B.: The primeval fireball today. *Am. Sci.* **57**(1), 37–74 (1969). (<https://www.jstor.org/stable/27828440>)
5. Partridge, R.B., 3, K.: The cosmic microwave background radiation. Cambridge University Press. **313**, (1995). <https://doi.org/10.1017/CBO97805115250703>
6. Durrer, R.: The cosmic microwave background: the history of its experimental investigation and its significance for cosmology. *Class. Quantum Grav.* **32**(12), 124007 (2015). <https://doi.org/10.1088/0264-9381/32/12/124007>
7. Tristram, M., Ganga, K.: Data analysis methods for the cosmic microwave background. *Rep. Prog. Phys.* **70**(6), 899 (2007). <https://doi.org/10.1088/0034-4885/70/6/R02>
8. Fixsen, D.J., Mather, J.C., Shafer, R.A., Brodd, S., Jensen, K.A.: The COBE/FIRAS Final Deliveries I: Data sets, improvements, and the cosmic and far infrared backgrounds. *American Astronomical Society Meeting Abstracts*, **191**, 91–05 (1997)
9. Shafer, R.A., Mather, J.C., Fixsen, D.J., Brodd, S., Jensen, K.A.: The COBE/FIRAS Final Deliveries II: The correlations and caveats relating galactic emission and the far infrared background. In: *American Astronomical Society Meeting Abstracts*, **191**, 91–06 (1997)
10. Smoot, G.F.: COBE observations and results. *AIP Conf. Proc. CONF 981098 Am. Inst. Phys.* **476**, 1–10 (1999). <https://doi.org/10.1063/1.59326>
11. Fixsen, D.J., et al.: Te cosmic microwave background spectrum from the full COBE FIRAS data set. *Astrophys. J.* **473**, 576–587 (1996). <https://doi.org/10.48550/arXiv.astro-ph/9605054>
12. Tsallis, C.: Possible generalisation of Boltzmann-Gibbs statistics. *J. Stat. Phys.* **52**, 479–487 (1988). <https://doi.org/10.1007/BF01016429>
13. Tsallis, C.: What are the numbers that experiments provide. *Quim. Nova* **17**(6), 468–471 (1994)
14. Tsallis, C.: Non-extensive thermostatistics: brief review and comments. *Phys. A: Stat. Mech. Appl.* **221**(1–3), 277–290 (1995). [https://doi.org/10.1016/0378-4371\(95\)00236-Z](https://doi.org/10.1016/0378-4371(95)00236-Z)
15. Tsallis, C., Cirto, L.J.: Black hole thermodynamical entropy. *Eur. Phys. J. C* **73**, 1–7 (2013). <https://doi.org/10.1140/epjc/s10052-013-2487-6>
16. Majhi, A.: Non-extensive statistical mechanics and black hole entropy from quantum geometry. *Phys. Lett. B* **775**, 32–36 (2017). <https://doi.org/10.1016/j.physletb.2017.10.043>
17. Czinner, V.G., Iguchi, H.: Rényi entropy and the thermodynamic stability of black holes. *Phys. Lett. B* **752**, 306–310 (2016). <https://doi.org/10.1016/j.physletb.2015.11.061>
18. Mejrhit, K., Ennadifi, S.E.: Thermodynamics, stability and hawking–page transition of black holes from non-extensive statistical mechanics in quantum geometry. *Phys. Lett. B* **794**, 45–49 (2019). <https://doi.org/10.1016/j.physletb.2019.03.055>
19. Boghosian, B.M.: Thermodynamic description of the relaxation of two-dimensional turbulence using Tsallis statistics. *Phys. Rev. E.* **53**(5), 4754 (1996). <https://doi.org/10.1103/PhysRevE.53.4754>
20. Rajagopal, A.K.: Dynamic linear response theory for a nonextensive system based on the Tsallis prescription. *Phys. Rev. Lett.* **76**(19), 3469 (1996). <https://doi.org/10.1103/PhysRevLett.76.3469>

21. Liu, Y.: Modifications of CMB spectrum by nonextensive statistical mechanics. *Eur. Phys. J. Plus* **137**(7), 1–11 (2022). <https://doi.org/10.1140/epjp/s13360-022-02974-3>
22. Sheykhi, A.: Modified Friedmann equations from Tsallis entropy. *Phys. Lett. B* **785**, 118–126 (2018). <https://doi.org/10.1016/j.physletb.2018.08.036>
23. Torres, D.F., Vucetich, H., Plastino, A.: Early universe test of nonextensive statistics. *Phys. Rev. Lett.* **79**(9), 1588 (1997). <https://doi.org/10.1103/PhysRevLett.79.1588>
24. COBE/FIRAS CMB Monopole spectrum: https://lambda.gsfc.nasa.gov/product/cobe/fras_monopole_get.html (2003). Accessed 5 Dec 2021
25. Khatri, R., Sunyaev, R.A., Chluba, J.: Mixing of blackbodies: entropy production and dissipation of sound waves in the early universe. *Astron. Astrophys.* **543**, A136 (2012). <https://doi.org/10.1051/0004-6361/201219590>
26. Choudhury, S.L., Paul, R.K.: A new approach to the generalization of Planck's law of black-body radiation. *Ann. Phys.* **395**, 317–325 (2018). <https://doi.org/10.1016/j.aop.2018.06.004>
27. Tsallis, C., Barreto, F.S., Loh, E.D.: Generalization of the Planck radiation law and application to the cosmic microwave background radiation. *Phys. Rev. E* **52**(2), 1447 (1995). <https://doi.org/10.1103/PhysRevE.52.1447>
28. Fixsen, D.J.: The temperature of the cosmic microwave background. *ApJ* **707**, 916–920 (2009). <https://doi.org/10.1088/0004-637X/707/2/916>
29. Biyajima, M., Mizoguchi, T.: Analysis of residual spectra and the monopole spectrum for 3 K black-body radiation by means of non-extensive thermostatics. *Phys. Lett. A* **376**(47–48), 3567–3571 (2012)
30. Beiser, A.: Concepts of modern physics, Tata McGraw-hill edition. 6th edn. **313**, (2008)
31. Stewart, S.M., Johnson, R.B.: Blackbody radiation: a history of thermal radiation computational aids and numerical methods. 1st edn, p. 414. CRC Press (2016). <https://doi.org/10.1201/9781315372082>
32. Bojarski, N.: Inverse black body radiation. *IEEE Trans. Antennas Propag.* **30**, 778–780 (1982). <https://doi.org/10.1109/TAP.1982.1142844>
33. Tikhonov, A.N., Arsenin, V.Y.: Solutions of ill-posed problems. Wiley, New York (1977)
34. Ye, J., et al.: The black-body radiation inversion problem, its instability and a new universal function set method. *Phys. Lett. A* **348**, 141–146 (2006). <https://doi.org/10.1016/j.physleta.2005.08.051>
35. Lakhtakia, M., Lakhtakia, A.: On some relations for the inverse blackbody radiation problem. *Appl. Phys. B: Photophysics Laser Chem.* **39**, 191–193 (1986). <https://doi.org/10.1007/BF00697419>
36. Chen, Nx.: Modified möbius inverse formula and its applications in physics. *Phys. Rev. Lett.* **64**, 1193 (1990). <https://doi.org/10.1103/PhysRevLett.64.1193>
37. Dou, L., Hodgson, R.: Maximum entropy method in inverse black body radiation problem. *J. Appl. Phys.* **71**, 3159–3163 (1992). <https://doi.org/10.1063/1.350957>
38. Wu, J., Ma, Z.: A regularized gmres method for inverse blackbody radiation problem. *Therm. Sci.* **17**, 847–852 (2013). <https://doi.org/10.2298/TSCI110316078W>
39. Wu, J., Zhou, Y., Han, X., Cheng, S.: The blackbody radiation inversion problem: a numerical perspective utilizing bernstein polynomials. *Int. Commun. Heat Mass Transf.* **107**, 114–120 (2019). <https://doi.org/10.1016/j.icheatmasstransfer.2019.05.010>
40. Konar, K., Bose, K., Paul, R.K.: Revisiting cosmic microwave background radiation using black-body radiation inversion. *Sci. Rep.* **11**, 1008 (2021). <https://doi.org/10.1038/s41598-020-80195-3>
41. Dhal, S., Paul, R.: Investigation on cmb monopole and dipole using blackbody radiation inversion. *Sci. Rep.* **13**, 3316 (2023). <https://doi.org/10.1038/s41598-023-30414-4>
42. Bernui, A., Tsallis, C., Villela, T.: Temperature fluctuations of the cosmic microwave background radiation: a case of non-extensivity? *Phys. Lett. A* **356**(6), 426–430 (2006). <https://doi.org/10.1016/j.physleta.2006.04.013>
43. Chluba, J., Sunyaev, R.A.: The evolution of CMB spectral distortions in the early universe. *Mon. Not. R. Astron. Soc.* **419**, 1294–1314 (2012)

Publisher's Note Springer Nature remains neutral with regard to jurisdictional claims in published maps and institutional affiliations.

Springer Nature or its licensor (e.g. a society or other partner) holds exclusive rights to this article under a publishing agreement with the author(s) or other rightsholder(s); author self-archiving of the accepted manuscript version of this article is solely governed by the terms of such publishing agreement and applicable law.